

Appendix contents

Supplementary Figures.....2

Supplementary Tables.....35

Supplementary Figure Legends

Figure S1. Expression pattern of cell-type specific AGO1 lines. **(A)** Columella; *ACR4::GFP:AGO1*. **(B)** Stele; *SHR::GFP:AGO1*. **(C)** Endodermis; *SCR::GFP:AGO1*. **(D)** Cortex; *CO2::GFP:AGO1*. **(E)** Epidermis; *WER::GFP:AGO1*. Scale Bars = 50 μ M.

Figure S2. Small RNA blot confirmation of RNA sequencing results. Input (left panels) and Immunoprecipitated (right panels) cell-type specific AGO1 probed for multiple different miRNA's listed on the right. NT(-) non-transformed with FLAG antibody added. NT(+) lysate were adjusted to $\sim \frac{1}{4}$ concentration and immunoprecipitated with native AGO1 antibody as a 'whole root' control. U6 is used as a loading control. The images used in the figures for the main text are repeated here. miR163, miR167, miR171 and miR173 are shown in Figure 1F. miR396 in Figure 4B. miR169 in Figure 5A. miR165/166 in Figure 6A.

Figure S3. RNA secondary structure of three new miRNA precursors. Structures were made using miRPlant software. Shown in red are the mature AGO1 loaded miRNA's.

Figure S4. Expression Pattern of HYL1 and specific effect of *hyl1-2* mutation on miRNA abundance. **(A)** Confocal images of two independent HYL1 translational fusions driven by the native promoter. **(B)** Representative miRoot browser snap shots of *HYL1* in WT and *hyl1* mutant. **(C)** RNA gel blot analysis of a set of hypomorphic miRNA biogenesis mutants. Probes are shown on the right and U6 serves as a loading control.

Figure S5. Polysome Profiling as a method to assay miRNA targeting. qRT-PCR on miRNA targets on total RNA from WT or *hyl1-2* mutants or total (35S) polysome immunoprecipitations on the same backgrounds. **(A)** *SPL10^{miR156}* **(B)** *TCP4^{miR319}* **(C)** *ARF17^{miR160}* **(D)** *CUC1^{miR164}* **(E)** *PHB^{miR165}* **(F)** *NF-YA2^{miR169}* **(G)** *MYB65^{miR165}* **(H)** *CSD2^{miR398}*. Error Bars represent +/- SD of three biological replicates.

Figure S6. Cell-type specific markers as assessed by polysome mRNASeq.

Normalized read counts of **(A) ACR4** **(B) SHR** **(C) SCR** **(D) CO2** **(E) WER** and **(F) GL2** in each cell-type specific polysome library. Values are the mean of two biological replicates from WT lines. Also shown are miRoot browser snapshots of representative transcripts.

Figure S7. Assembly of the miRoot brower. To facilitate single-cell exploration

of the root-tip's miRNA biology, the F:AGO1-IP and F:RPL18-IP sequencing datasets were integrated into a user-friendly browser coined [miRoot](#), designed to operate on desk computers, tablets or smartphones. Cell-specific signals for single miRNAs (WT background) or single mRNA translomes (WT/*hyl1-2* backgrounds) are queried in miRoot via a virtual root interface where colored patterns of various intensities reflect the relative pan-layer signals' strengths. The interface was designed by graphic cell layer deconvolution (Adobe Illustrator) based upon authentic high-resolution photographs of WT versus *hyl1-2* root tips, as depicted in **(A)**. The virtual root depictions therefor take into account the characteristics of *hyl1-2* compared to WT root-tips, including cellularly disorganized columella and quiescent center, enlarged stele, and defects in the anticlinal-versus-periclinal division rates of epidermal cells. The layers were then digitalized and assembled to reconstitute the virtual root interfaces. In the **miRNA-query** miRoot setting shown in **(B)**, blue square on the top), all currently known Arabidopsis miRNAs (miRbase v.21) may be interrogated primarily via their numeric identifier; the plethora of new miRNAs discovered in this study, isomiRs and targets thereof will be incorporated at later stages. Upon miRNA query, all known matching miR-5p/3p and paralogs (a, b, c, d...) are displayed in a pulldown menu alongside the sequence of the mature miRNA guide strand (blue rectangle). We stress that miRoot displays signal intensities for AGO-loaded *i.e.* functional miRNAs, that are relative to one another between cell layers. The cross-layer signals of the miR156 isoform **a**, strand **5p** are depicted here as an example. Root images are exported in an Adobe Illustrator® CS6-compatible format via the save option (blue square).

In the **transcript-query** miRoot setting shown in **(C)**, blue square on the top), the full, curated Arabidopsis transcriptome (TAIR10) may be interrogated via gene

identification number (e.g. *AT1G69170* here), gene describer (e.g. SBP-domain transcription factor) or gene name (e.g. *SPL6*). In its most simplified implement, miRoot can thus be used as a root-tip layer-specific translatome analyzer. We have verified that its performances are at least on par with those of the cell-specific root translatome available from the [eFP bowser](#) (Bailey-Serres group at UCR). All plant miRNA targets predicted and/or validated so far display extended miRNA:target site complementarity such that they constitute a highly predictable subset of the Arabidopsis transcriptome. In the example shown in **(C)** the miR156 target *SPL6^{miR156}* was queried and, thus, the colored maps obtained in **(A)** for the miR156**a** and **(C)** for *SPL6^{miR156}* can be compared visually. Here mutually-exclusive patterns of AGO1-loaded miR156a, on the one hand, and *SPL6^{miR156}* accumulation on the other, are observed, as expected from a direct, cell-autonomous plant miRNA-target interaction. Note that the stele signals do not show, however, this mutually-exclusive pattern and this will be addressed in points **F**-onward.

miR156 belongs to an extended family of paralogs (**a-b-c-d-e-f-g-h-i**) displaying each single-nucleotide polymorphisms that may refine targeting of specific SPL transcripts. Some of these paralogs are much less expressed and loaded into AGO1 than others, however, yet miRoot will display layer-specific patterns regardless of signal intensity. This might be confusing when visually analyzing the respective contributions of isoforms to target regulation as illustrated in panel **(D)** with miR156**a** signal and miR156**g**. The raw values (squared in blue) show that the signal intensity for paralog **a** is two-orders-of magnitude higher than that of paralog **g**. The scale option (blue square and inlay) solves this issue by allowing signal normalization between any number of miRNA paralogs subjected to the option, with the values being recalculated relative to the paralog displaying the highest-intensity signal. Panel **(E)** illustrates how rescaling highlights the near-background AGO1-loading signal of miR156 paralog **g** across root cell layers. Signal rescaling of all miR156 paralogs likewise identified that, in addition to **g**, paralogs **h** and **I** have no significant contribution to root-tip gene regulation (not shown). miR156 paralogs **a-b-c-d-e-f-g** display similar AGO1-loading signals in each root-tip layer, and since they are all involved, in principle, transcript targeting, it might be desirable to measure their bulk contribution to *SPL6^{miR156}* regulation in each cell layer. As shown in **(F)** miRoot allows signal accretion via

the “add to sum-group” option (the blue rectangle shows that any miRNA paralog can be selectively removed from the sum-group at any time). A “Sum-Group” is then generated (blue rectangle, top right corner) upon which the “create” option allows signal aggregation in each individual layer, as depicted here in the grey zone for miR156**a-b-c-d-e-f-g**. Note that signal accretion can also be useful to reconstitute the inferred bulk regulation conferred by paralogous miRNA displaying distinct spatial AGO1-loading patterns and/or different signal intensities. It was used, for instance, in this study, with miR164**a/b** and miR164c as shown in fig. S10C.

Importantly, miRoot also enables removal of single/multiple layers and concurrent re-calculation of relative signal intensities across the remaining cell files. This option notably enables exclusion of the stele, of which none of the four intrinsic layers was individually resolved by SHR:F::AGO1-IPs, as discussed in the main text. miRoot will thus artificially assign often elevated and single-layer signals to the other stele layers. Because the stele represents a major fraction of the root, this can create exaggerated signals potentially masking/undermining those of adjacent cell files, since all signals are relative to each-others. (**F-G**) illustrate this phenomenon with elevated stele-derived signals from each miR156 paralogs **a-f** (~35,000 Normalized read counts/paralog, panel B) resulting, upon accretion, in a total signal of ~213,000 Normalized read counts (panel F, blue square). As shown in (**G**, blue rectangle), these elevated signals barely contribute to *SPL6^{mir156}* transcript regulation in the whole stele (1.3 folds-change in *hyl1* versus WT). Accordingly, no significant change in *SPL6^{mir156}* accumulation is observed in the stele in the WT compared to *hyl1* backgrounds (**C**). This suggests that the strong stele miR156 signals originate mainly from a single, as yet undefined stele cell-type, and are diluted in the others. By contrast, for instance, the epidermis-derived miR156**a-f** signals (green square), contribute significantly to *SPL6^{mir156}* control in this layer, given the 4.5 folds-change in *hyl1* versus WT transcript accumulation observed (**G**). Panel (**H-I**) shows how the stele removal option used on both the miR156**a-f** (**H**) and *SPL6^{mir156}* (**I**) miRoot outputs resolves the caveat and provides, upon recalculation of relative signal intensities across all adjacent layers, a more accurate view of the spatial *SPL6^{mir156}* regulation. In particular, the epidermal miR156 **a-f** pool now clearly stands out as the dominant

contributor to this spatial regulation (compare **B-C** to **H-I**). These adjustments thereby contribute to refine the mutually-exclusive pattern observed initially (**B-C**). As expected, the *SPL6^{mir156}* translatome signal is elevated in all layers in the *hyl1* background, and in the epidermis in particular. This optional layer-removal feature is also useful to focus analyses of layer-specific regulations, as was done in the case of *GRF2* regulation by miR396a (Figure 3H-J).

Figure S8. Contrasted loading of miR and miR* across cell-layers. Brower snapshot of miR824-5p (miR) and miR824-3p (miR*) demonstrating differential loading across different cell types.

Figure S9. Cell-type specific regulation of MYB transcription factors by miR159. **(A)** Layer-specific normalized read counts of miR159 paralogs a-b-c from AGO1-IP-deep-Seq and independent northern analysis. Lower panel: scaled, layer-specific AGO1-IP signal of each miR159 paralog and sum thereof calculated via miRoot **(B)** Representative confocal images of *pmiR159a::H2B::GFP* and *pmiR159b::H2B::GFP* transcriptional fusions. **(C)** Representative confocal images of *pMYB33::H2B::GFP* and *pMYB65::H2B::GFP* transcriptional fusions. **(D)** miRoot snapshots of layer-specific translatome signals for *MYB33* (left) and *MYB65* (right) in WT versus *hyl1* backgrounds. **(E)** Expression pattern of *MYB33* genomic fusion in WT or *hyl1* backgrounds. **(F)** Relative expression of *MYB33* as assessed by qRT-PCR in different cell types after cell-type specific polysome immunoprecipitation in WT and *hyl1* backgrounds. The top graph represents raw values per cell layer and on the bottom adjusted for each cell layer with WT for each set at 1 and mutant adjusted relatively within each cell layer. **(G)** The same as shown in (F) but for *MYB65*. **(H)** Generic scheme demonstrating the principles of miRNA-mediated buffering. Scale bars represent 50µM. Error bars represent +/- SD of two biological replicates. The same blot in panel A is shown in Figure 1F.

Figure S10. miR397-directed regulation of Lac4 across contiguous developmental stages.

(A) Representative confocal images of *LAC4* transcriptional (left) and translational (right) fusions. MZ,TZ,EZ,DZ: meristematic, transition, elongation,

differentiation zone. **(B)** miRoot snapshots of layer-specific translatome signals for *LAC4*. **(C)** Scheme demonstrating special and temporal miRNA-mediated gene regulation revealed by cell-type specific profiling. Scale bars: 50 μ M. Polysome signals are Log values of reads per 10 million, and AGO1-IP miRNA values are normalized read counts.

Figure S11. Selective expression gradients of miR164 family targets dictated by limiting miRNA concentration **(A)** Confocal images of *pmiR164a::mVENUS-N7* (left), *pmiR164b::H2B:GFP* (middle) and *pmiR164c::mVENUS-N7* (right). **(B)** Normalized miR164a-c read counts and independent northern analysis. **(C)** Browser snapshot of AGO1:miR164a-b (left) and miR164c (right) accumulation. **(D)** Endodermis and cortex focused accumulation of miR164 paralogues a-b (left), c (centre) and sum of the two is shown on the right. **(E)** Browser snapshots of total polysome transcripts for NAC1 in WT and *hyl1* mutants. **(F)** The same as shown in (D) but for NAC6. **(G)** Focused miRoot analysis of the *NAC1* translatome signal in WT versus *hyl1* endodermis/cortex and predicted sequence alignment between miR164a/b-c and *NAC1* (target). **(H)** Same as (G) but for NAC6. **(I)** Representation of principles of gene regulation mediated by gradients and base-pairing of miRNA:target combinations across cell layers. A portion of the blot shown in Figure S2 is shown here in panel (B) *: statistically significant upregulation based on two biological replicates with a fdr of <0.05. Scale bars represent 50 μ M. All miRNA levels are represented as Normalized read counts per million and Polysome sequencing is shown as LOG(RP10M).

Figure S12. Translational repression of GRF's by miR396 in the columella. **(A)** miRoot browser images of *GRF3* polysome profiling in WT and *hyl1* highlighting only the Columella. Also shown is the normalized read count values for each background. **(B)** Expression of translational fusion of either WT *GRF3* (left) or resistant (*rGRF3*-right) GFP reporters. **(C)** MiRoot browser images of *GRF1* polysome profiling in WT and *hyl1* highlighting only the Columella. Also shown is the normalized read count values for each background. Scale for miRoot are LOG(ReadsPer10Million) and the graphs are normalized read counts. **(D)**

MiRoot browser snapshot of *PLT2* transcript levels within the Columella. Error bars are +/- SD of two biological replicates. Scale bars represent 50 μ M.

Figure S13. Non-cell autonomous accumulation and activity of miR165/166.

(A) Normalized read counts of miR165 and miR166. Representation of the sum of miRNA165a/166b accumulation. **(B)** Confocal images of miR165a and miR166b transcriptional activity. miRoot browser snapshots in WT and *hyl1* mutants of miR165/166 targets **(C)** *PHV* **(D)** *REV* and **(E)** *AtHB15*. Log scales (RP10M) are shown.

Figure S14. Non-cell autonomous accumulation and activity of miR160 (A)

Representative confocal images of *pmiR160(a/b/c)::H2B::GFP* transcriptional fusions. **(B)** Northern analysis of AGO1-loaded miR160. **(C)** miRoot snapshots of layer-specific translatome signals for *ARF173* in WT versus *hyl1* backgrounds.

Figure S15. Maintenance of cell specific and autonomous AGO1 accumulation and molecular confirmation of miR395 induction upon Sulfur starvation. (A) Cell-type specific expression of *GFP::AGO1* translational fusions upon SO₄⁻ starvation **(B)** Western blot analysis of miR395 transcriptional reporter lines under normal (+) and SO₄ starvation (-) conditions. Coomassie blue (CB) staining serves as a loading control **(C)** RNA gel blot analysis of RNA from the same roots sampled in (B) showing induction of miR395 under each experimental condition. U6 serves as a loading control. Scale Bars represent 50 μ M.

Figure S16. Non-cell autonomous activity of miR395. miRoot browser shots of miR395 targets **(A)** *APS4* **(B)** *APS1* **(C)** *SULTR2;1* in WT and *hyl1* backgrounds. Scales are LOG values of RP10M.

Figure S17. Binding miRNA duplexes within the epidermis. (A) *pWER::GFP:P19* confocal image demonstrating the cell-autonomy of P19 within the epidermis. **(B)** Western blots of two independent IPs that were performed corresponding to; left the RNA used in (C) and right RNA used in (D). Coomassie

Blue (CB) serves as a loading control for the input. **(C)** RNA gel blot analysis of IPed epidermal specific guide strand miRNAs as indicated by the probes of the right. U6 serves as a loading control for the input. **(D)** RNA gel blot analysis of independently IPed epidermal specific star (*) strand miRNAs as indicated on the right and also the guide strand for miR396. U6 serves as a loading control for the input. Scale bar represents 50 μ M.

Fig. S18. Sequestering miR395 by Stele specific P19 expression. **(A)** Western blot analysis of *pSHR::HA:P19* IPs under normal (+) and sulfur starved conditions (-). Coomassie blue (CB) staining serves as a loading control for the input. **(B)** RNA gel blot analysis of *pSHR::HA:P19* IPs under normal (+) and sulfur starved conditions (-). miR159 serves as a negative control for SO₄- specific induction of miR395 and U6 serves as a loading control. The images in (B) are also used in Figure 7.

Figure S19. Expression and movement of pri/miRNA163. **(A)** Confocal images of *pmiR163::H2B:mCHERRY*. **(B)** Brower shots of polysome bound primiR163 in either WT (left) or *hyl1*. **(C)** Brower shot of mature miR163 accumulation. Scale bars represent 50 μ M. Scales for browser images are Normalized read counts.

Figure S20. Movement of miR160 within mature leaf tissue. **(A)** Cross section of leaf and the cell types isolated using the meselect technique. Vasculature is circled and lower epidermis is shaded in red. **(B)** Western blot analysis of whole leaf and meselect separated vasculature and epidermis. Two independent lines each of *pmiR160a::H2B:GFP*, *pmiR160b::H2B:GFP* and *pmiR160c::H2B:GFP* are shown. After GFP detection the membrane was stripped and detection of ACTIN2 was performed to demonstrate that protein isolated using the technique were amenable to antibody detection. Coomassie blue (CB) serves as a form of loading control. **(C)** RNA gel blot analysis of whole leaf, vasculature or epidermis isolated from either WT or *hyl1* mutant plants. Probes are given on the right and U6 serves as a loading control. Note some of portions of this figure are the same images as shown in the main text as Figure 7.

Figure S21. Promoter activity of APS4. *pAPS4::H2B:GFP* transcriptional fusions in either WT or *hyl1* backgrounds under either normal (SO₄+) or Sulfur starvation conditions (SO₄-) are shown.

Table S1. Mapping statistics for deep sequencing of cell-type specific AGO1 bound miRNAs.

Table S2. Normalized Read counts for all known miRNAs in cell-type specific AGO1 libraries.

Table S3. List and statistics of new miRNAs identified in cell-type specific AGO1 libraries.

Table S4. Mapping statistics for RNAseq of cell-type specific polysome bound mRNAs in WT and *hyl1* backgrounds.

Table S5. Differential analysis of RNAseq of cell-type specific polysome bound mRNAs in WT and *hyl1* backgrounds.

Table S6. List of oligonucleotides used in this study.

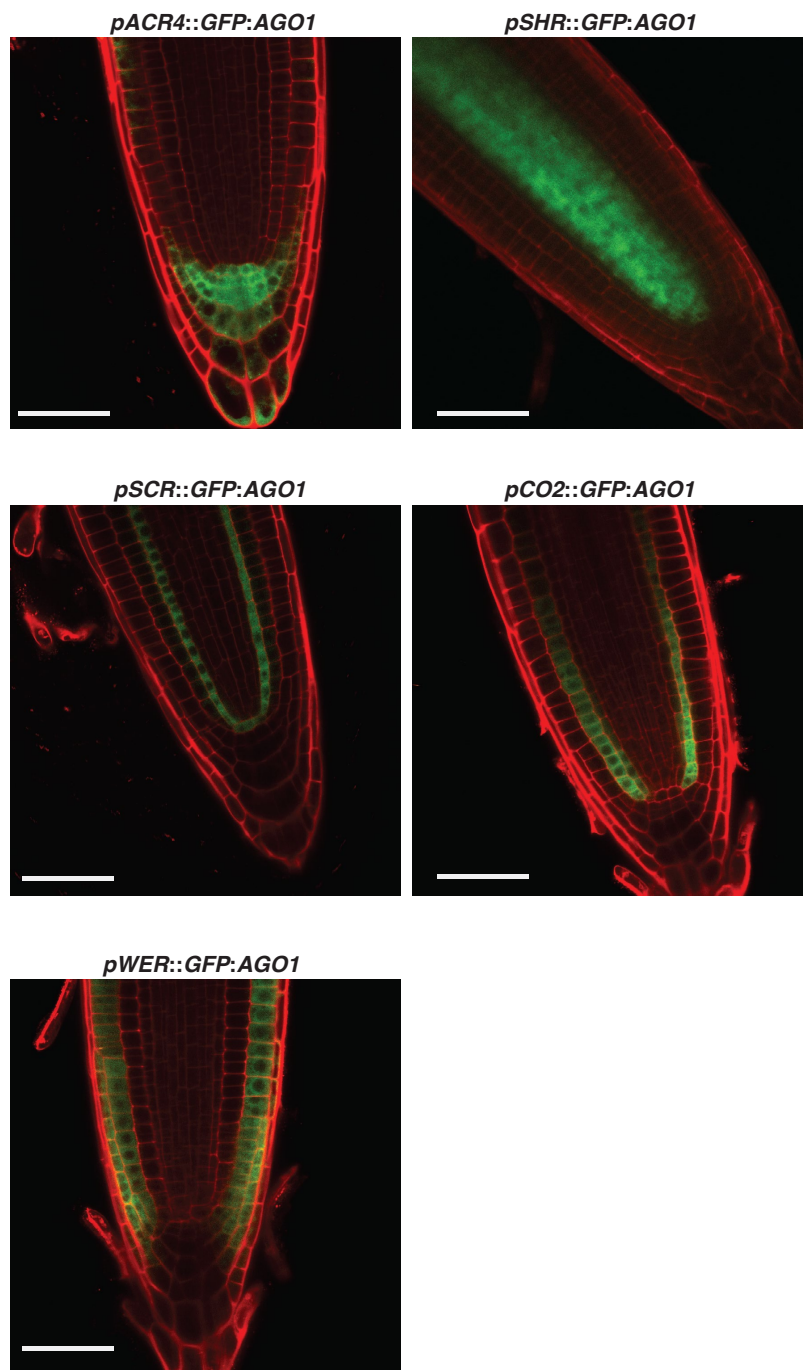


Figure S1

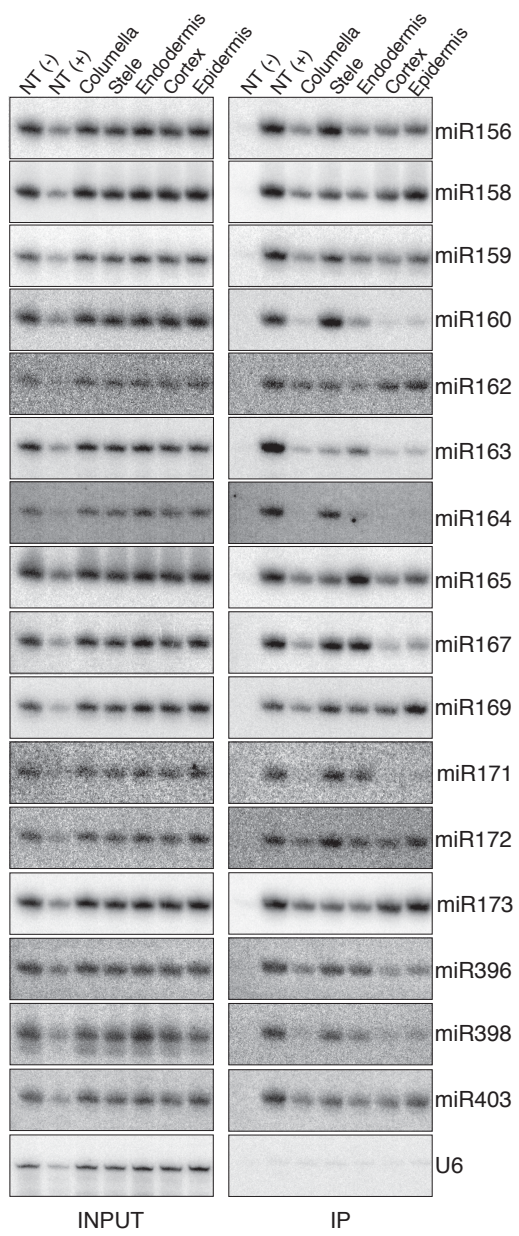


Figure S2

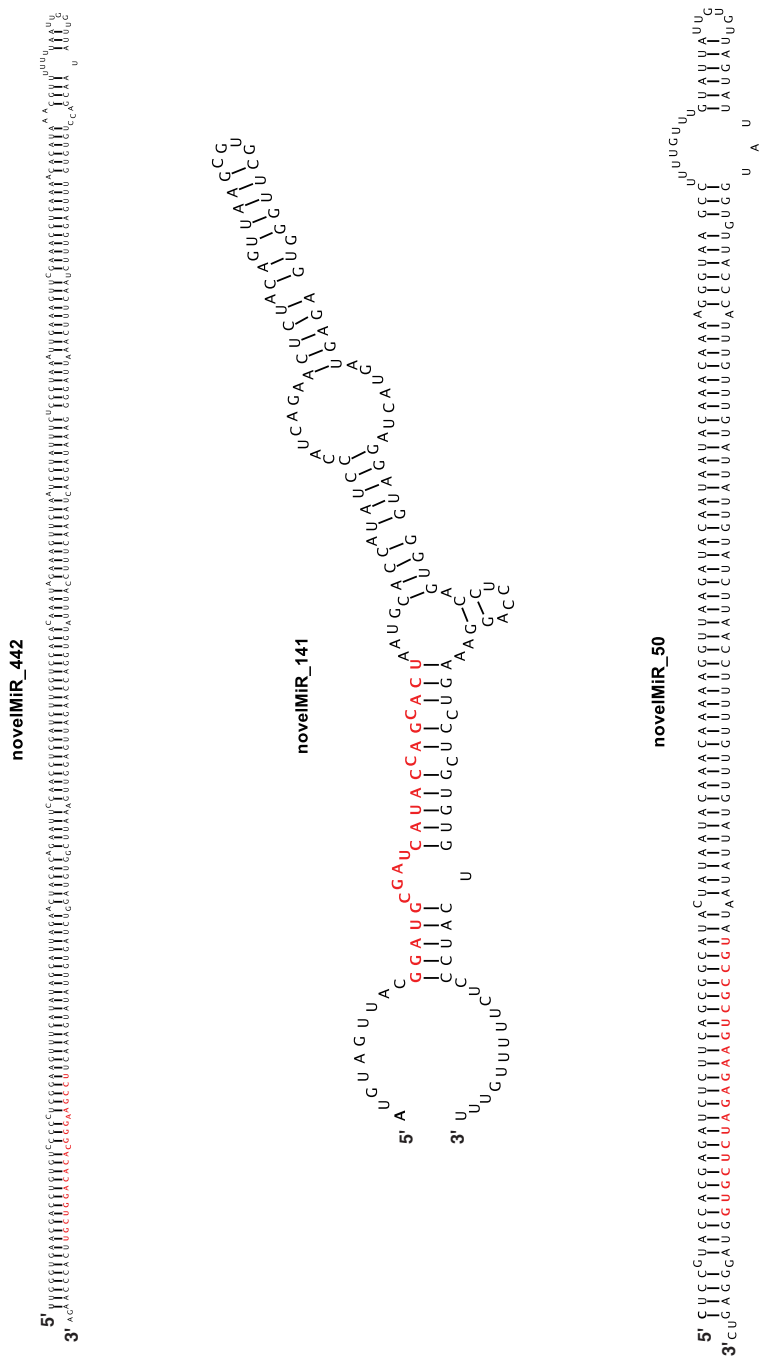


Figure S3

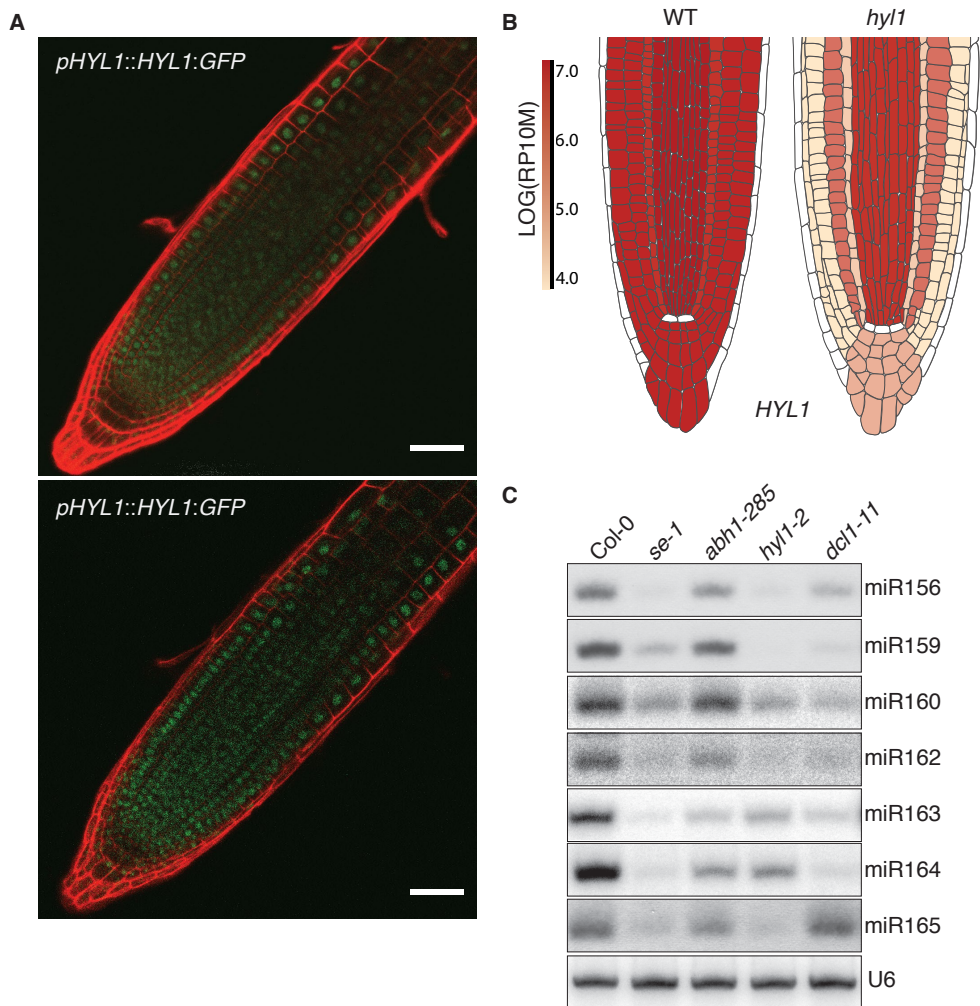


Figure S4

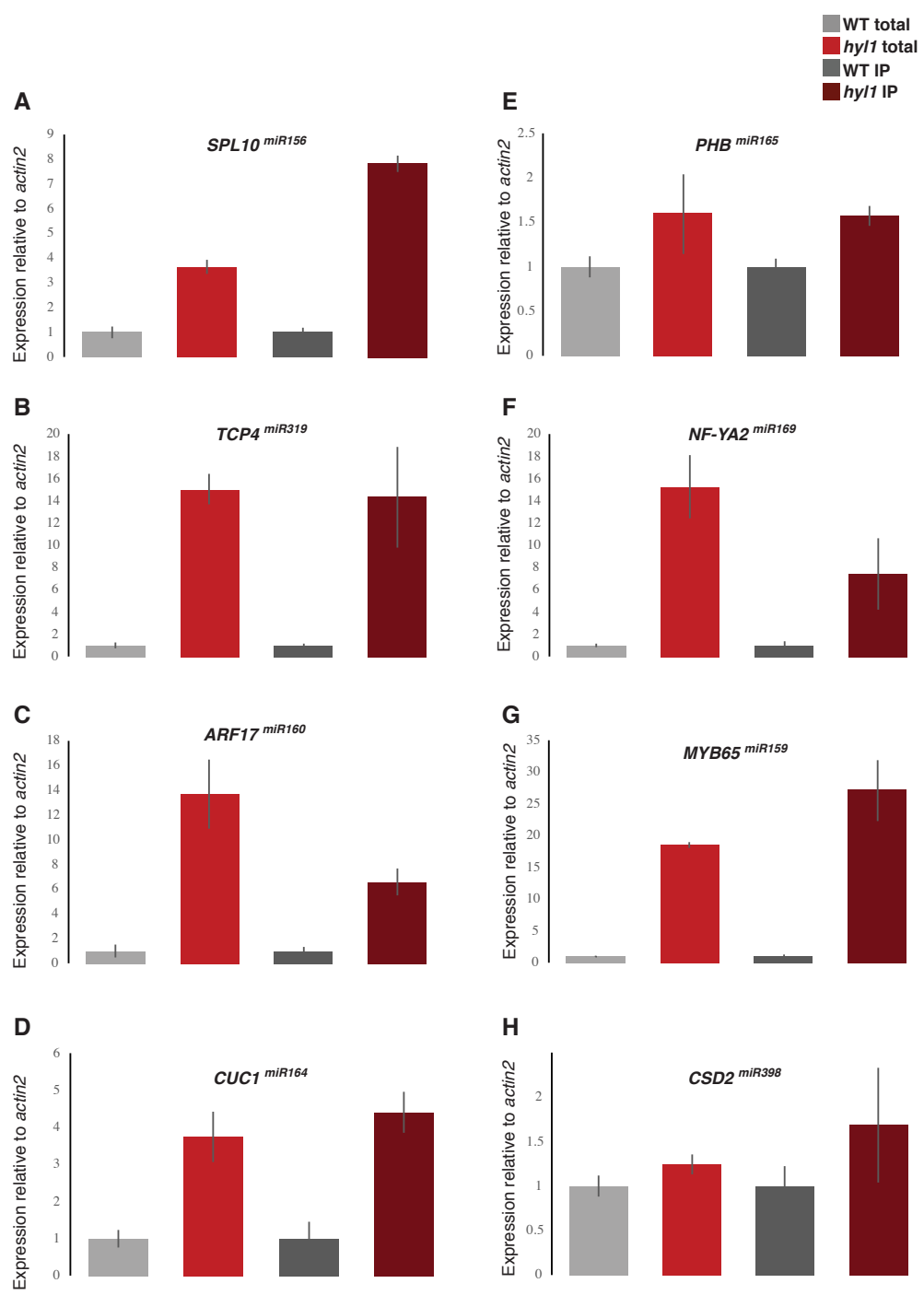


Figure S5

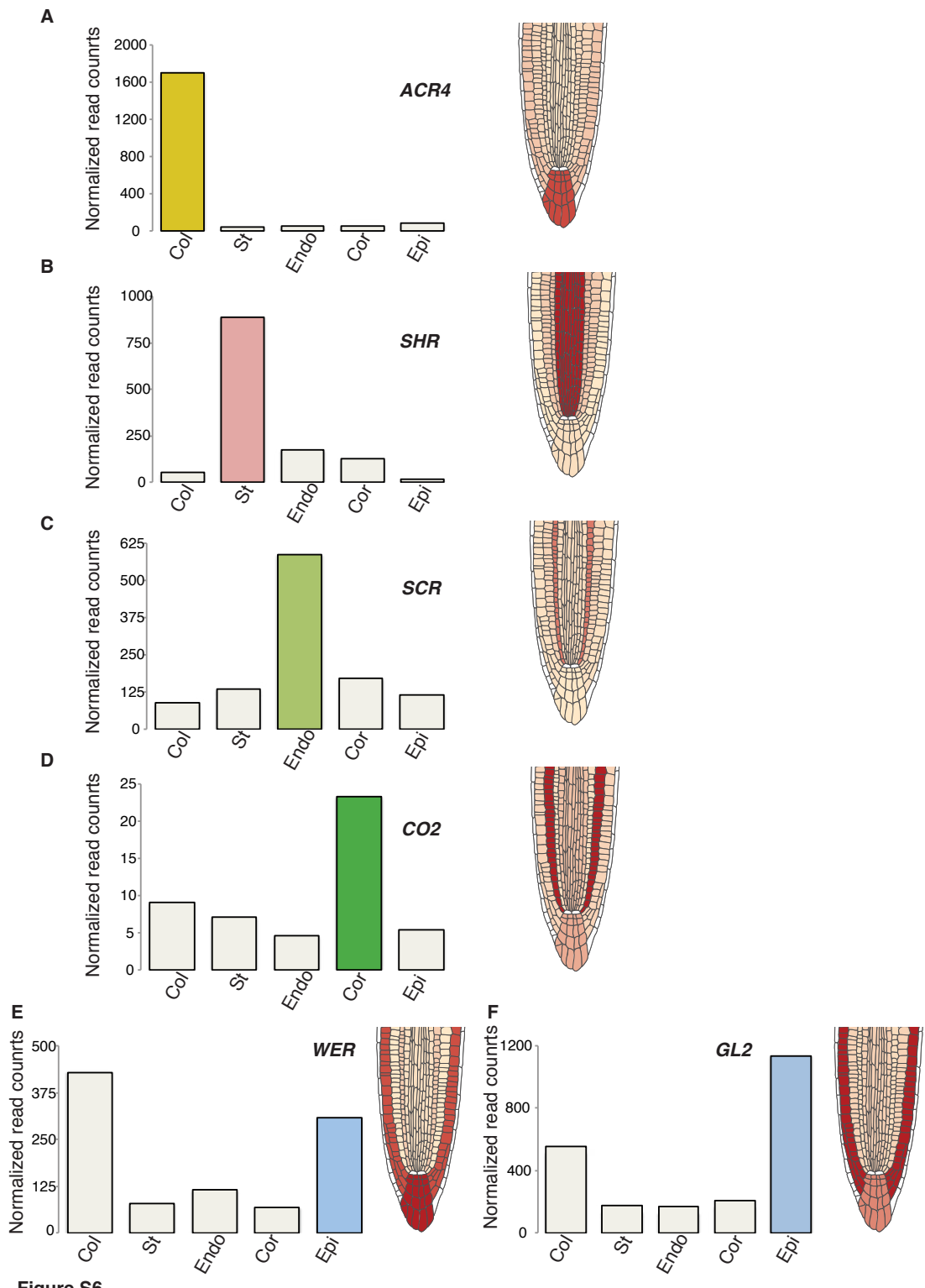


Figure S6

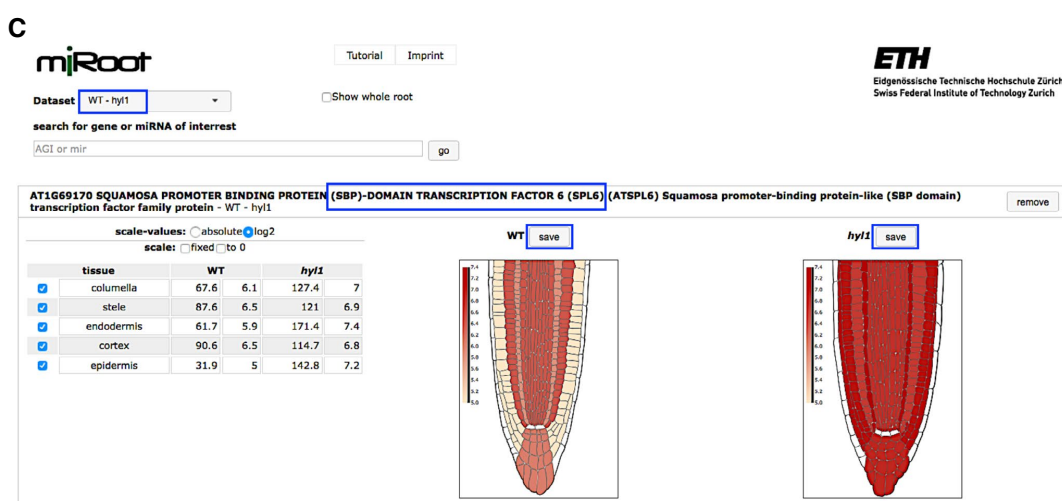
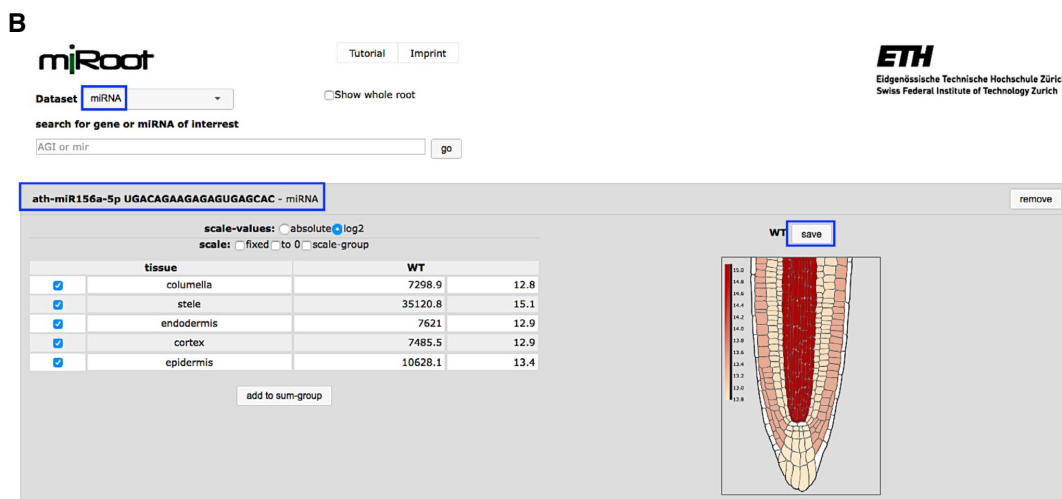
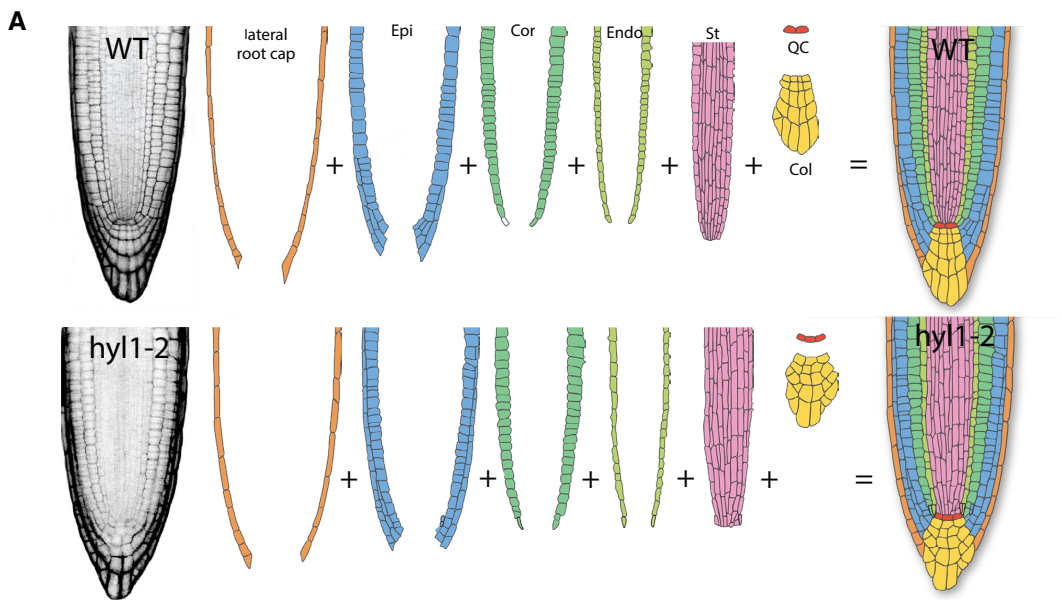


Figure S7 (continued on next page)

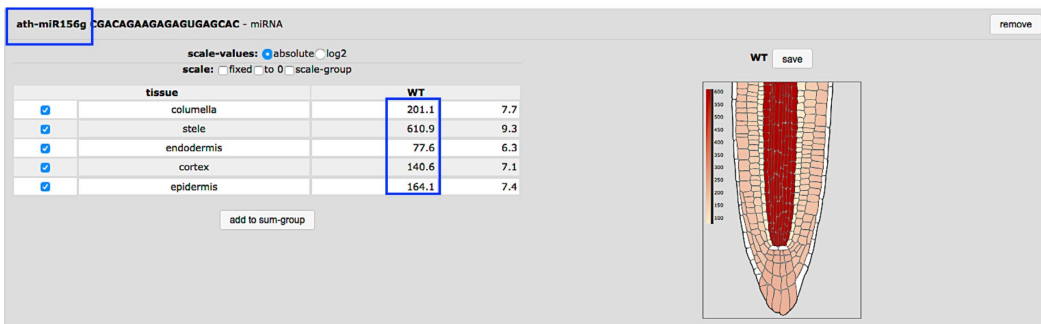
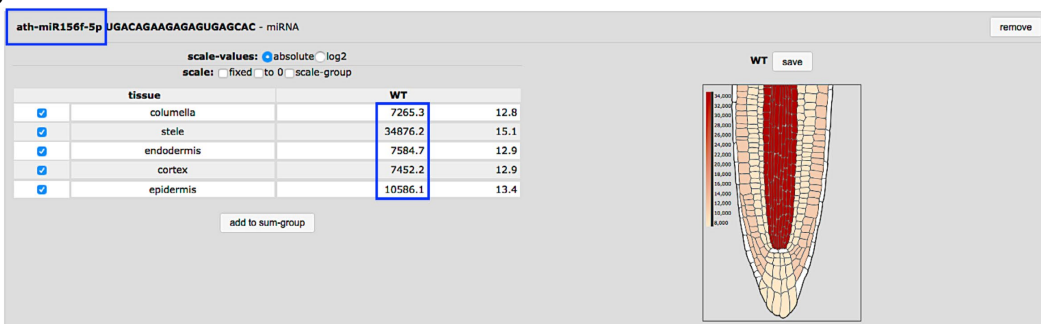
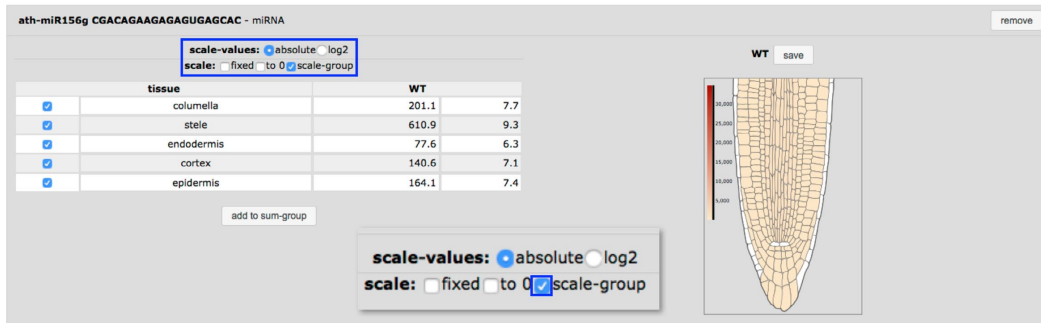
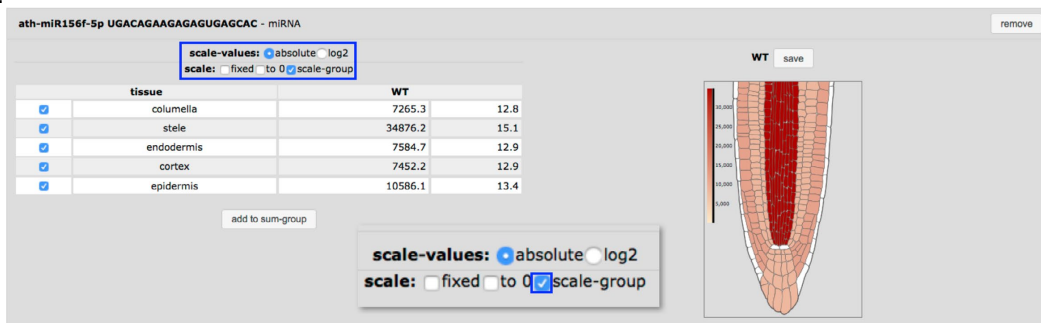
D**E**

Figure S7 (continued on next page)

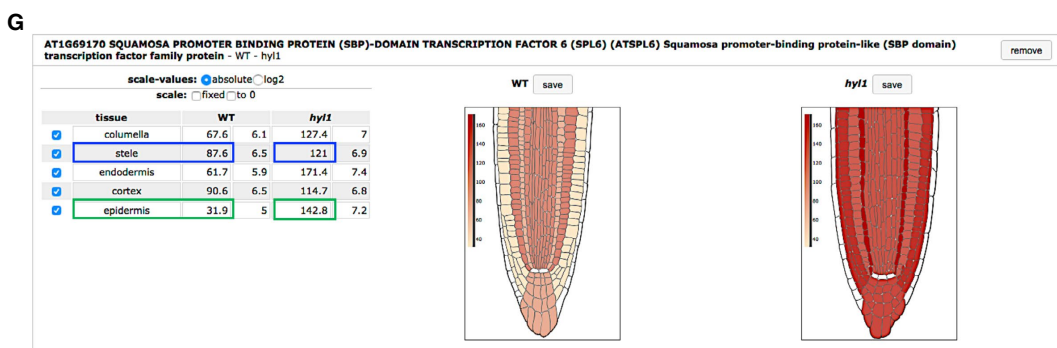
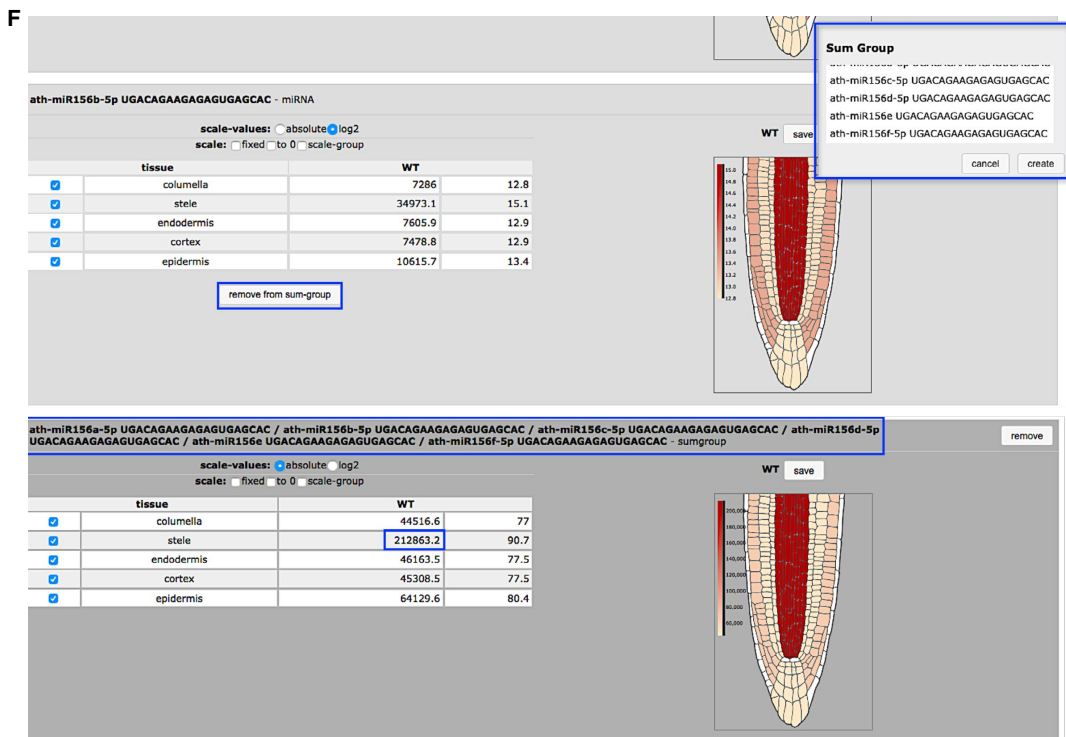


Figure S7 (continued on next page)

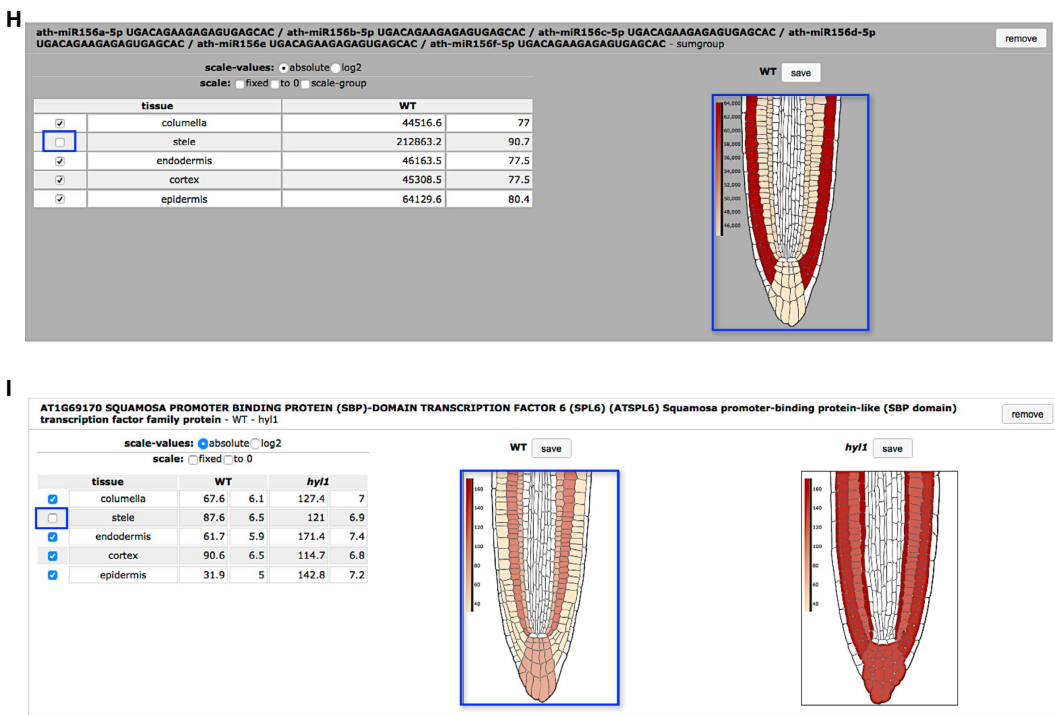


Figure S7

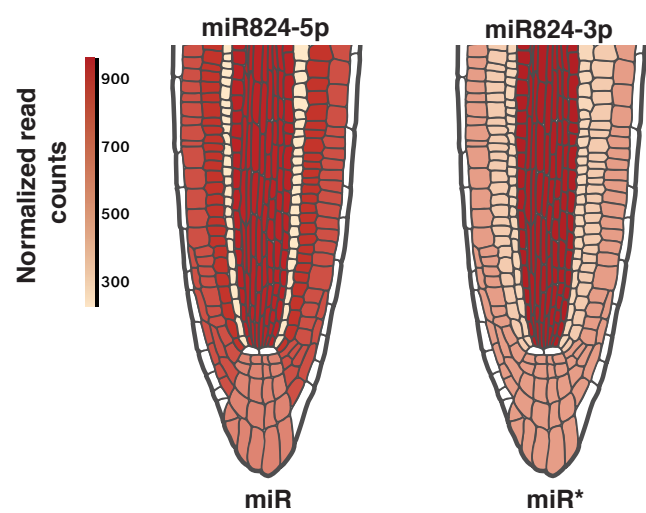


Figure S8

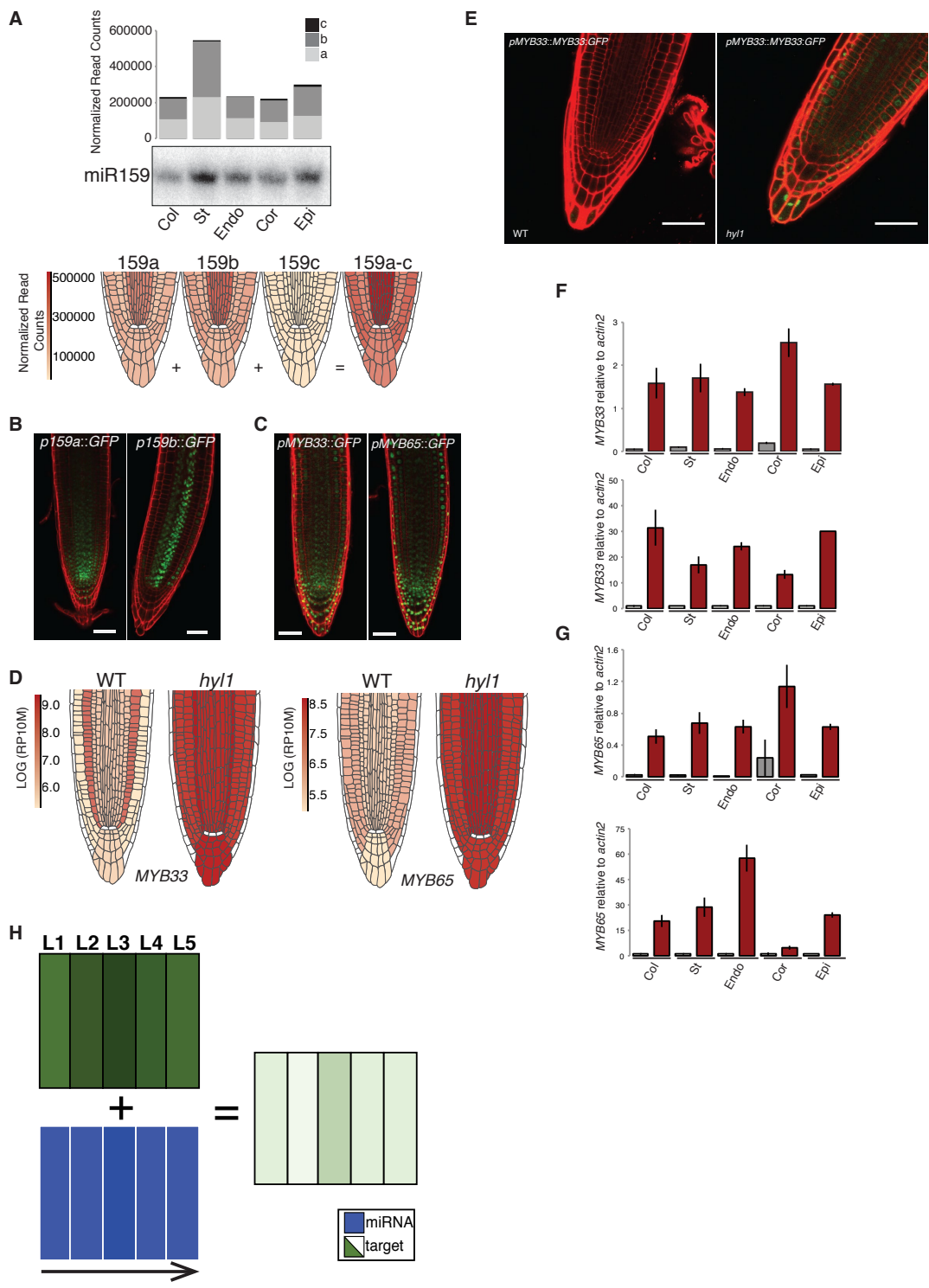


Figure S9

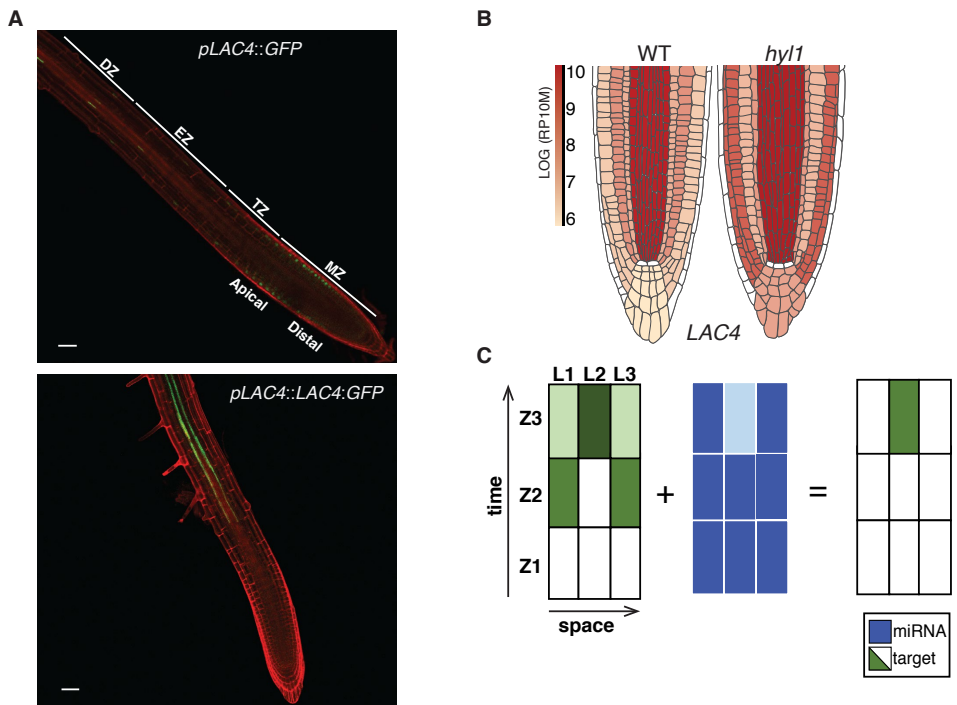


Figure S10

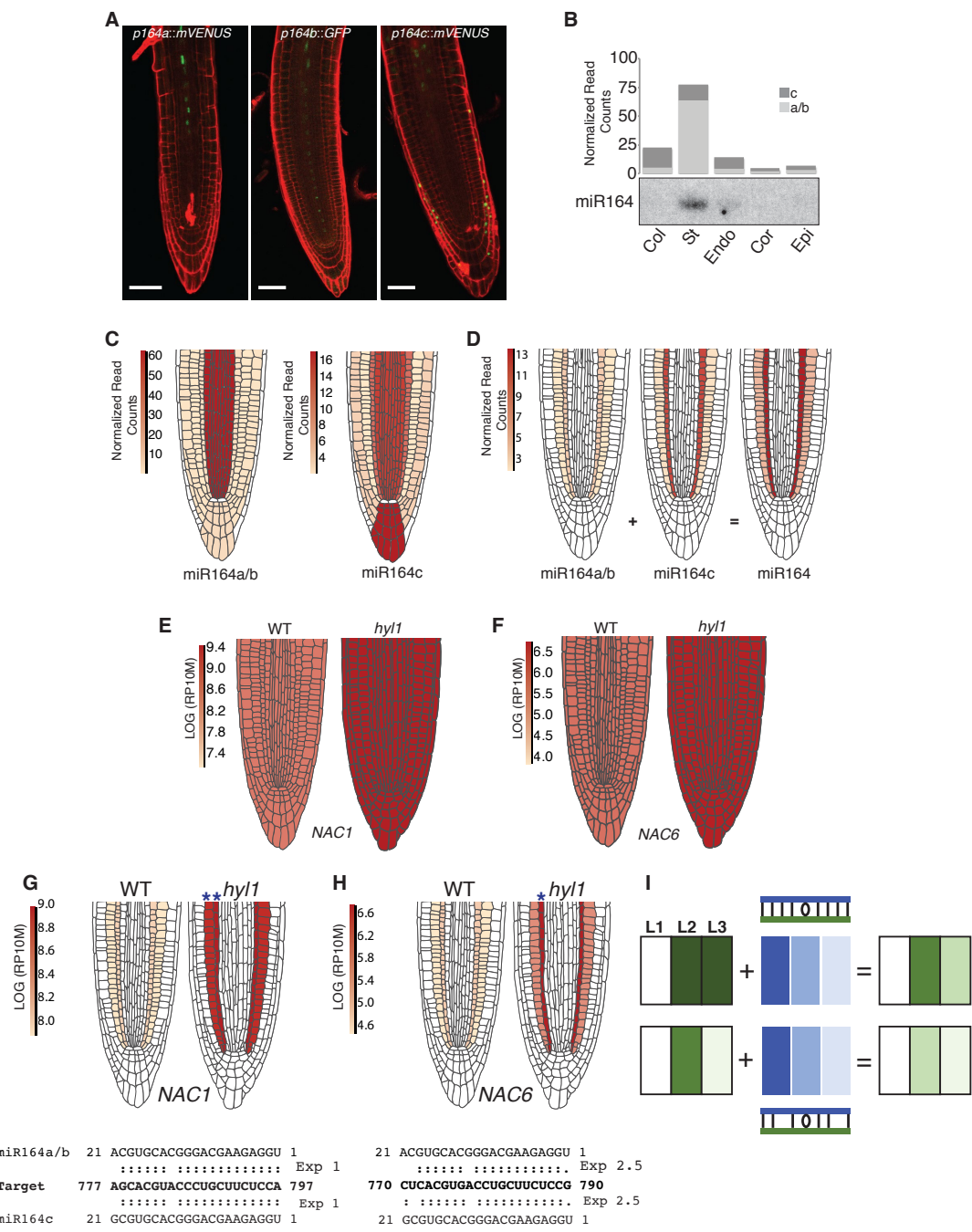


Figure S11

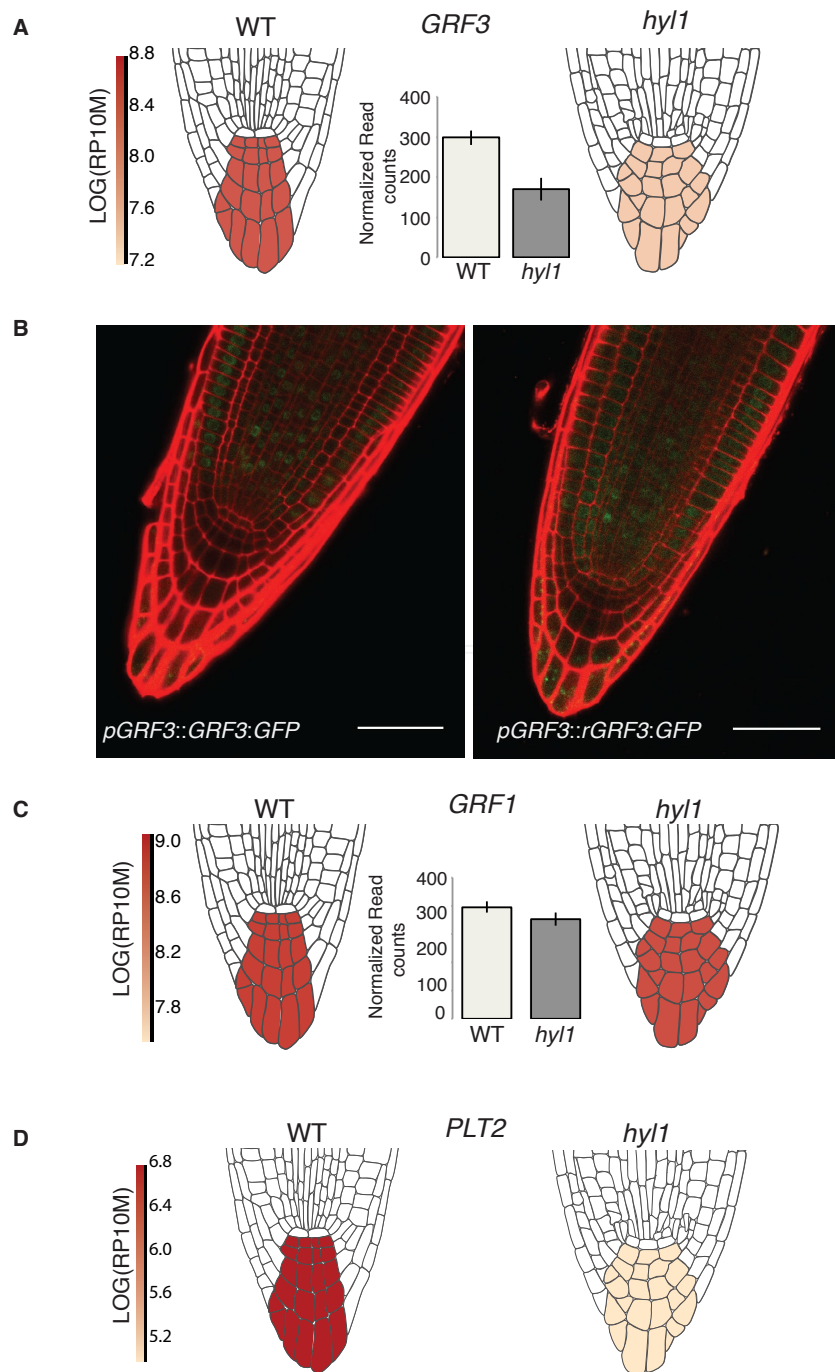


Figure S12

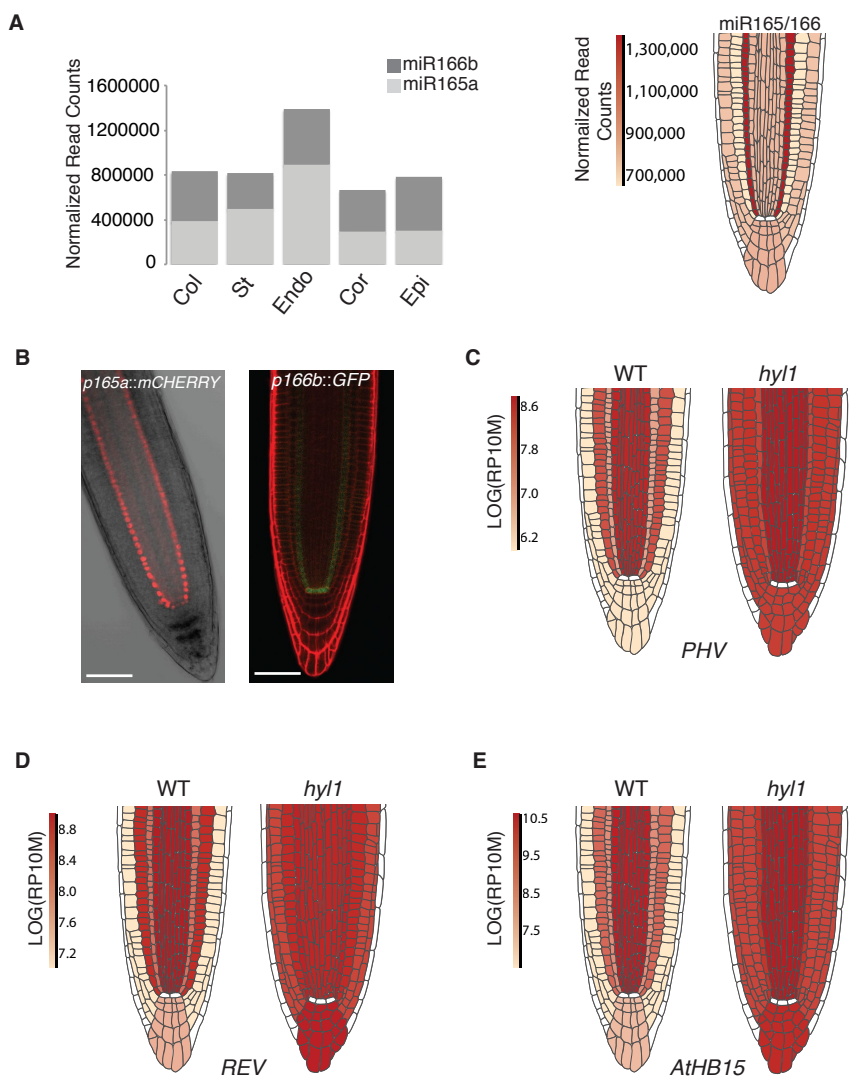


Figure S13

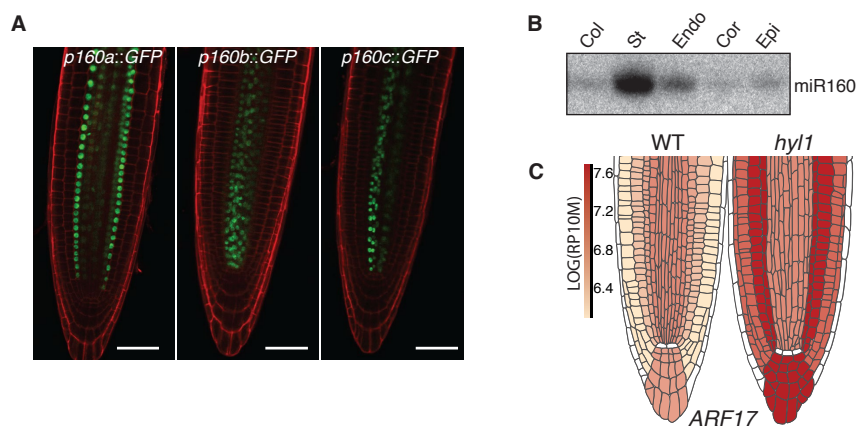


Figure S14

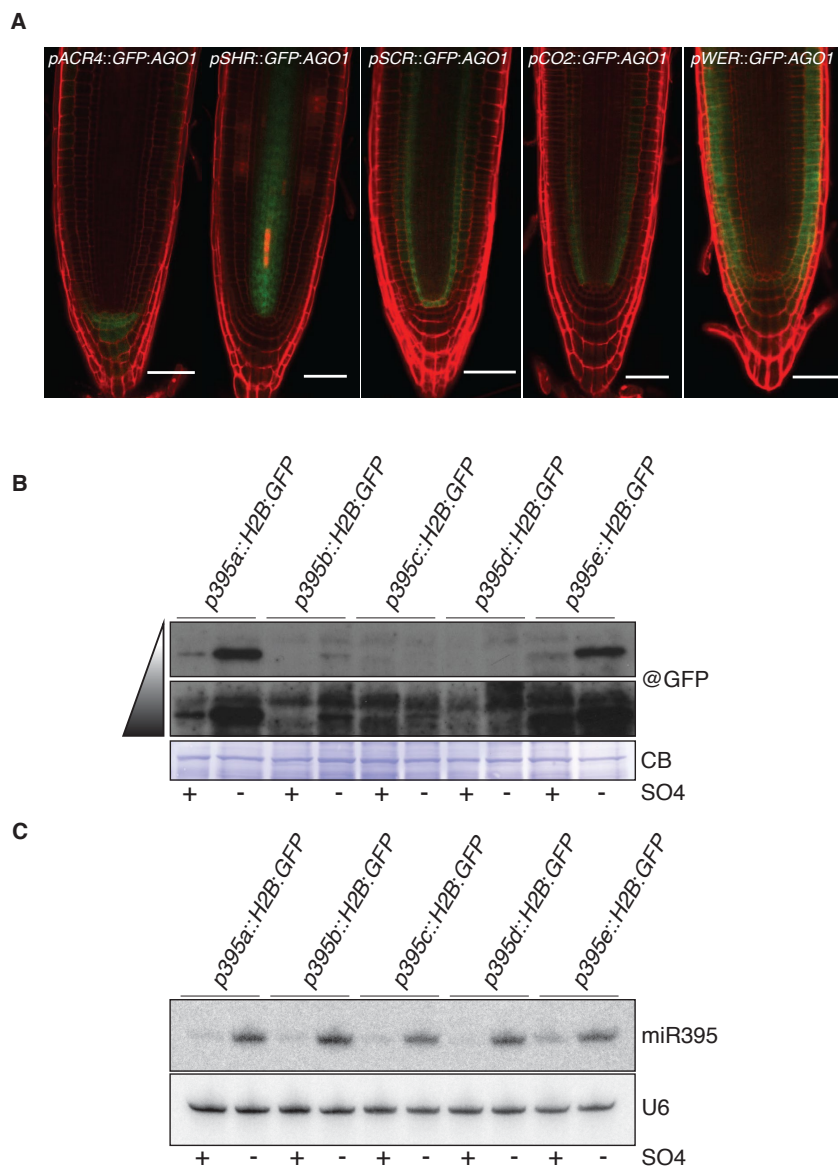


Figure S15

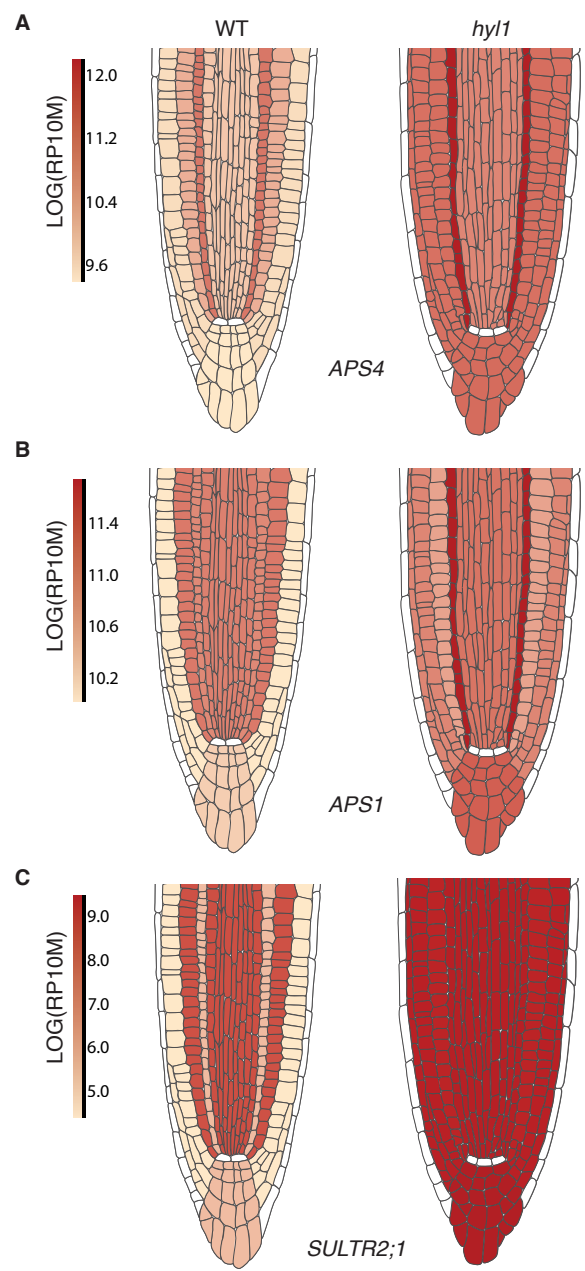


Figure S16

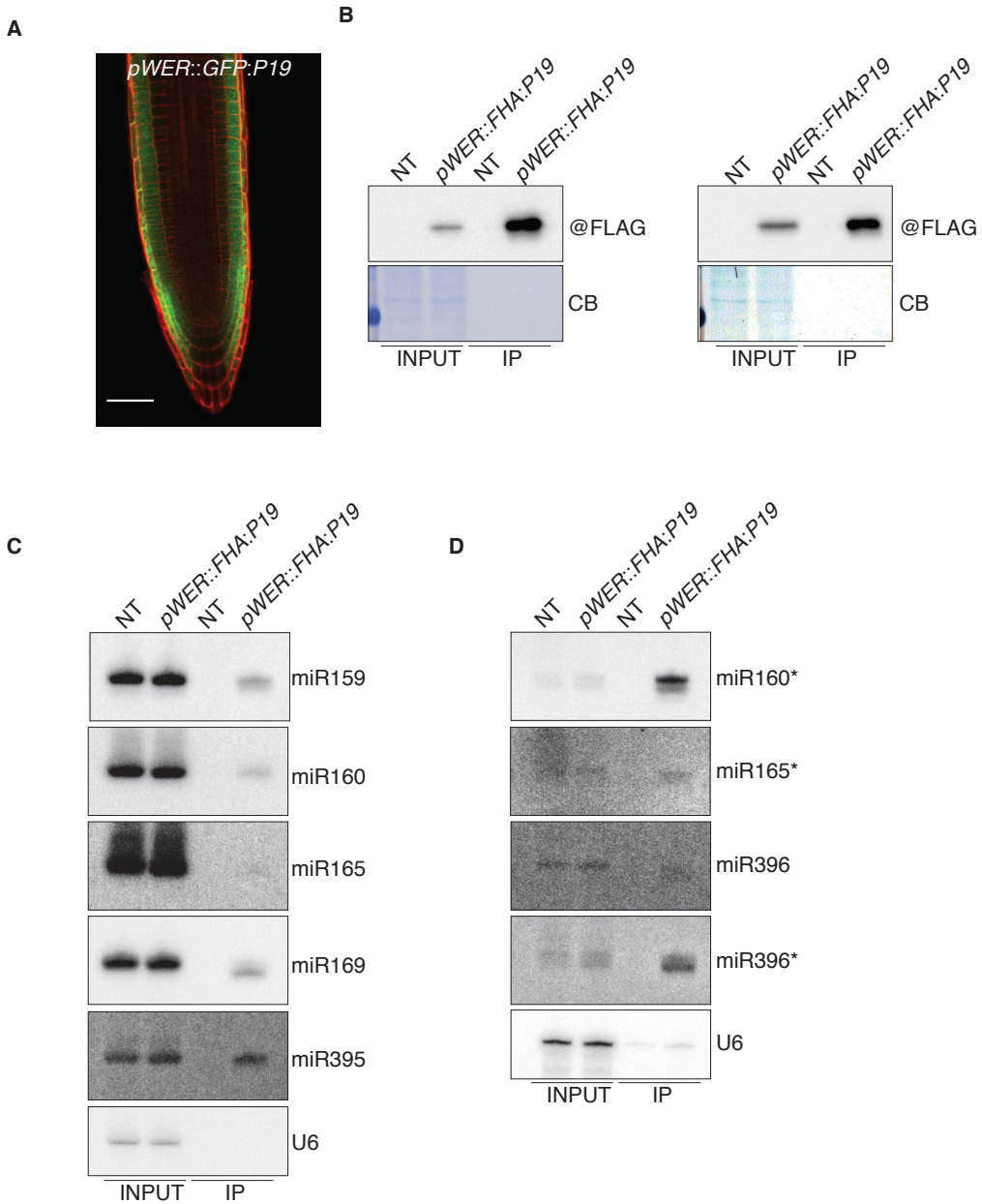


Figure S17

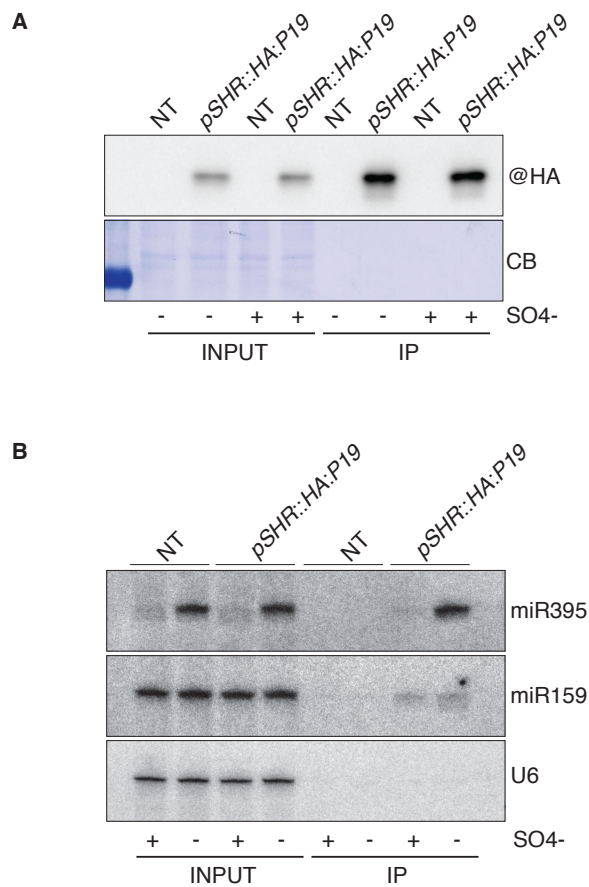


Figure S18

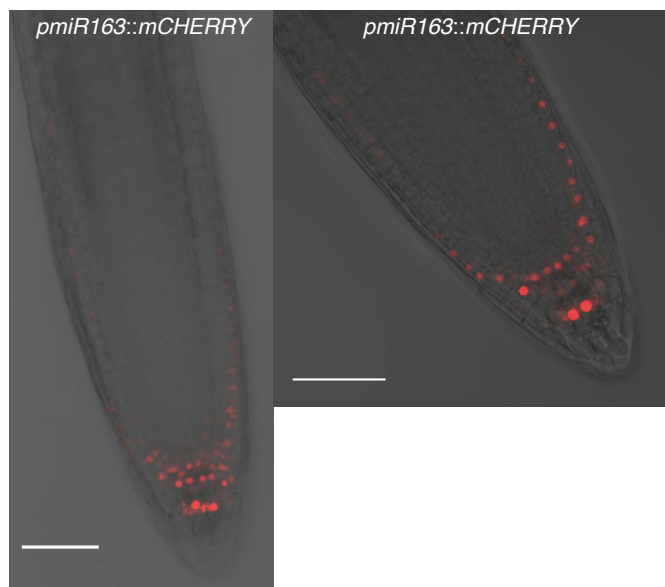
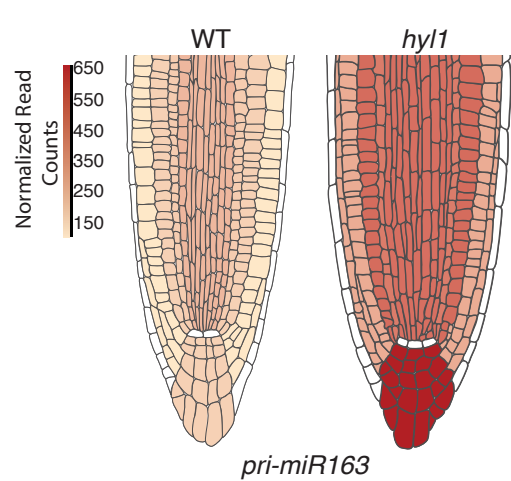
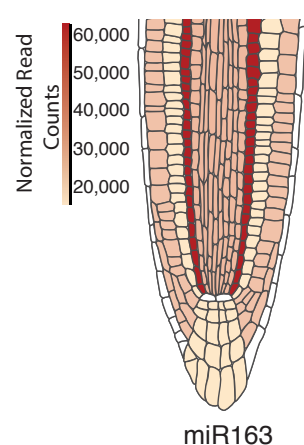
A**B****C**

Figure S19

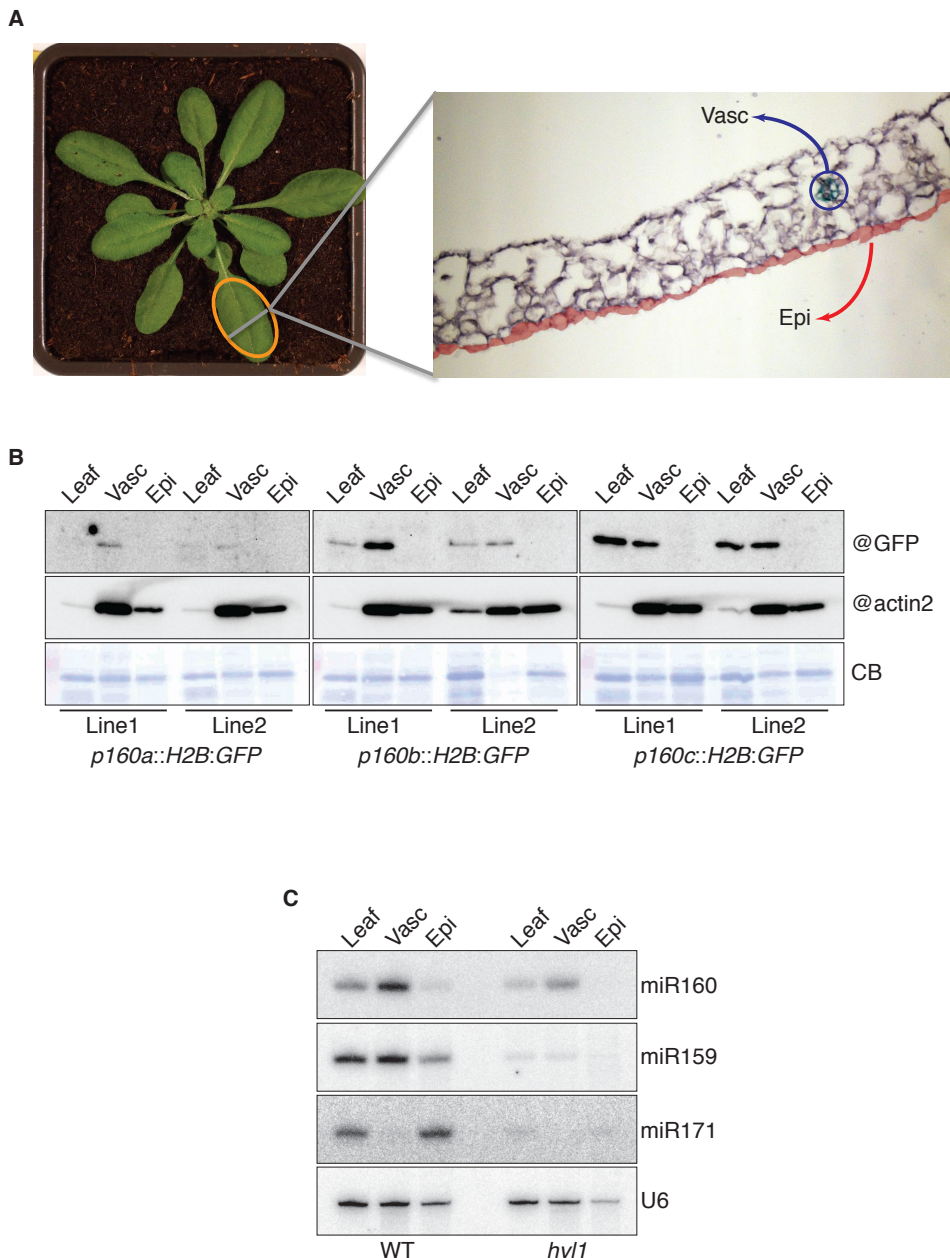


Figure S20

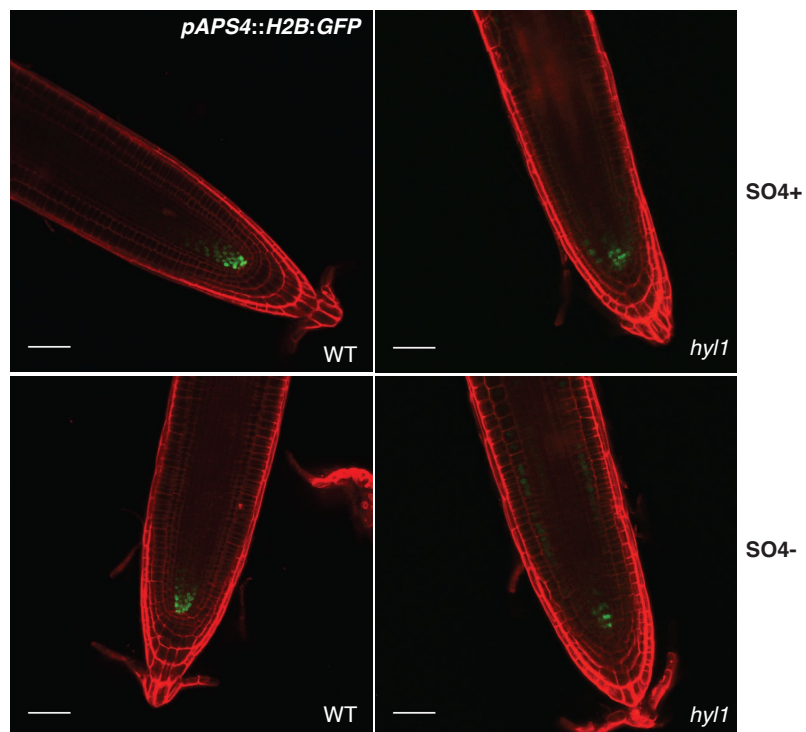


Figure S21

Appendix Table 1

lib	'aw reads 15-	# mapped reads	% mapped reads	IRNA precursor	reIRNA precursor reads
GYK.2(AGO1)	18547490	16799853	90.58	13492335	80.31
GYK.3(ACR4)	17599135	15522843	88.20	10168756	65.51
GYK.4(SHR)	24998562	21453974	85.82	17461625	81.39
GYK.5(SCR)	21787779	19595676	89.94	15709545	80.17
GYK.6(CO2)	19666086	16409688	83.44	11956425	72.86
GYK.7(WER)	29909684	25655350	85.78	19796913	77.16

Appendix Table 2

Appendix Table 3

Appendix Table 4

lib	# pairs	Aligned pairs	concordant pair alignment rate
GMD223b	1696652	1447578	84.80%
GMD224b	2743027	2406198	87.10%
GMD225b	3092823	2675710	85.90%
GMD226b	2221055	1930868	86.30%
GMD227b	1991982	1744233	86.60%
GMD228b	3410932	3061744	89.20%
GMD229b	3917449	3447302	87.30%
GMD230b	2978900	2640463	87.90%
GMD231b	4043314	3347378	82.20%
GMD232b	3405071	2983312	86.80%
GMD233b	1991940	1698903	84.80%
GMD234b	2971257	2500468	83.70%
GMD235b	2453424	1875648	75.70%
GMD236b	2808082	2428328	85.70%
GMD237b	2668505	2160672	80.20%
GMD238b	1936080	1660909	84.70%
GMD223	2393973	2064037	85.60%
GMD224	4874636	4263659	86.80%
GMD225	2673809	2312224	85.90%
GMD226	2927919	2533901	85.90%
GMD227	4394680	3819099	86.20%
GMD228	4114742	3653711	88.10%
GMD229	3313899	2912220	87.10%
GMD230	3394558	2955665	86.20%
GMD231	3495667	2955958	83.80%
GMD232	3572938	3138549	87.00%
GMD233	2939881	2547790	86.00%
GMD234	3046494	2665706	86.80%
GMD235	2980596	2382646	79.00%
GMD236	2793329	2442720	86.50%
GMD237	3388022	2878677	84.00%
GMD238	2949176	2575866	86.30%
GMD320	1572214	1273663	80.10%
GMD321	2325149	1801879	76.80%
GMD322	2167765	1656935	75.80%
GMD323	2140760	1658761	76.70%
GMD89	6068297	4752216	77.60%
GMD90	6220116	5407906	86.30%
GMD91	7041616	5355730	75.30%
GMD92	7552573	6054558	79.20%

NAME	SEQUENCE
Pro-ACR4-4-F	GGGGCAACTTGTATAGAAAAGTGGAAATAGTCAGAAATGCC
Pro-ACR4-1-R	GGGGCTGTTTTGTACAAACTTGTCAAAGCACACACCGC
Pro-ACR4-1-F	GGGGACAAGTTGTACAAAAAAGCAGGCTATAGCAAGAAATGCC
Pro-ACR4-2-R	GGGGACCACTTGTACAAGAAAGCTGGTCAAAGTCACACACACGC
Pro-SHR-4-F	GGGGCAACTTGTATAGAAAAGTGGATCAGAGCGTGGGTTCTTC
Pro-SHR-1-R	GGGGCTGTTTTGTACAAACTTGTGAGAAAGGGAGACCCACAATATC
Pro-SCR-4-F	GGGGCAACTTGTATAGAAAAGTGGATAAGTGGAAATTACCTGGA
Pro-SCR-1-R	GGGGCTGTTTTGTACAAACTTGTGGCGTGAGATTGCATGGTA
Pro-CO2-4-F	GGGGCAACTTGTATAGAAAAGTGGACTAACTCATTATTACGACTG
Pro-CO2-1-R	GGGGCTGTTTTGTACAAACTTGTAAACTCTGTTGCATTATTGTC
Pro-WER-4-F	GGGGCAACTTGTATAGAAAAGTGGATGATCTAACGACGAAACG
Pro-WER-1-R	GGGGCTGTTTTGTACAAACTTGTGTTCTTGATGATGAGAC
Pro-WER-1-F	GGGGACAAGTTGTACAAAAAAGCAGGCTCTGATCTAACGACGAAACG
Pro-WER-2-R	GGGGACCACTTGTACAAGAAAGCTGGGTTGTTCTTGATGATGAGAC
Pro-159A-NI-F	AAGCGGCCGCCCTATCAACAAAGTTGGG
Pro-159A-BHI-R	AAGGATCCCTCCATCGTCAGATCAAGATCTATCG
Pro-159B-NI-F	AAGCGGCCGCCGAAAAGGGTTCTAGGTTATCTCGCGAAAG
Pro-159B-XhoI-R	AACTCGAGTCTTCTTCCTTGTGTTCTATATAATCG
Pro-160A-NI-F	ACGCGGCCGCCATTGTGAATAATATTCAACAAAGGAAG
Pro-160A-SpeI-R	ACACTAGTCATATGTATATGCGTCATGAC
Pro-160B-NI-F	ACGCGGCCCGTAACAGTATTATGATGTTATGG
Pro-160B-SpeI-R	ACACTAGTATGTATACGGGAACCCCT
Pro-160C-NI-F	ACGCGGCCGCTGTAATAGTGTGCGGTGTTG
Pro-160C-BHI-R	ACGGATCCGTATACCAACCTCTACGCATG
Pro-163-4-F	GGGGCAACTTGTATAGAAAAGTGGATGAGATCATCCAAATATATCGT
Pro-163-1-R	GGGGCTGTTTTGTACAAACTTGTGGGTTGGTGTATTATCT
Pro-164B-NI-F	CCGCGGCCGCGAACGTTAACGTGTATTGTAC
Pro-164B-BHI-R	CGCGGATCCTCTTGCTCATCACACACCTTC
CB-pro165a-4-F	GGGGACAACCTGTATAGAAAAGTGTGTCAGTCATGGATTTT
CB-pro165a-1-R	GGGGACTGCTTTGTACAAACTTGGGTGTTATGATGAGGGAAT
Pro-395A-NI-F	TCAGCGGCCGCTTGACTCTCTTGTAGCT
Pro-395A-Xho-R	TCACTCGAGCCAACCAAGAATATTGTTTC
Pro-395B-NI-F	TCAGCGGCCGCCAACCAAGAATATTGTTTC
Pro-395B-XhoI-R	TCACTCGAGTTGACTCTCTTGTAGCT
Pro-395C-NI-F	TCAGCGGCCGCCGGGGACTCTGGTGTATTGTAC
Pro-395C-XhoI-R	TCACTCGAGTACAAACAACTAACACTG
Pro-395D-NI-F	TCAGCGGCCGCGCTAAATGCTTATATTGT
Pro-395D-BHI-R	TCAGGATCCATCTAGTCGAATTATTATTG
Pro-395E-NI-F	TCAGCGGCCGCCGTGGGATTGAAAAGATGC
Pro-395E-BHI-R	TCAGGATCCTGAAAAAGAATGGAGGGACT
Pro-396A-4-F	GGGGCAACCTGTATAGAAAAGTGGATTCCCTGTCTGTTG

Pro-396A-1-R	GGGGCTGTTTGTACAAACTTGTAGGGTCATGTAGAGCAGACG
Pro-396B-4-F	GGGGCAACTTGTATAGAAAAGTGGAGGTTGTGTTTATCGC
Pro-396B-1-R	GGGGCTGTTTGTACAAACTTGTGGATCTCATCTCCCTC
Pro-397A-4-F	GGGGCAACTTGTATAGAAAAGTGGAGTGGCAAGTCTATTACCGAA
Pro-397A-1-R	GGGGCTGTTTGTACAAACTTGTAAACCAGGAAAAATATCCT
Pro-397B-4-F	GGGGCAACTTGTATAGAAAAGTGGACAAATGTGGAAATCATCTC
Pro-397B-1-R	GGGGCTGTTTGTACAAACTTGTCAAGGGAAAAATATCTCC
Pro-MYB33-NI-F	GAGCGGCCGCGAAAGCCTCCGGCACAGCA
Pro-MYB33-SpeI-R	GAACTAGTCTCTTCTAATTAAACCACTG
Pro-MYB65-NI-F	GAGCGGCCGCGAGTGGACAAGTTAAAGATG
Pro-MYB65-HIII-R	GAAAGCTCTCTTCTACTTAAAGCAAGAC
Pro-GRF2-4-F	GGGGCAACTTGTATAGAAAAGTGGATAATTGAGTTGTCAAAAAACTCCTTTATATTACTTACTT
Pro-GRF2-1-R	GGGGCTGTTTGTACAAACTTGTAAAGAAGTAATATAAAAAG
Pro-Lac4-NI-F	GAGCGGCCGACGCATATTGTATGTAGCC
Pro-LAC4-BHI-R	GAGGATCCCTCCCTCTCTATCTTCTCT
CB-proAPS4-F	GGGGCAACTTGTATAGAAAAGTGGACAAATATGTAAACTATTAGA
CB-proAPS4-R	GGGGCTGTTTGTACAAACTTGTGATTAATCAGTTTTTG
Pro-HYL1-NotI-F	CAGCGGCCGCAATATGAGCCCAGTCCCT
Pro-HYL1-BHI-R	CAGGATCCCTGAATTAAATTCAAACC
MYB33-CDS-1-F	GGGGACAAGTTGTACAAAAAAGCAGGCTTATGAGTTACACGAGCACTGAC
MYB33-CDS-2-R	GGGGACCACTTGTACAAGAAAAGCTGGGTCTCCGGTAGTTCTGTATTTGAC
GRF2-CDS-1-F	GGGGACAAGTTGTACAAAAAAGCAGGCTCATGGATATTGGTGTTC
GRF2-CDS-2-R	GGGGACCACTTGTACAAGAAAAGCTGGGTCTCCGGTTGTAAATGAAAG
LAC4-CDS-1-F	GGGGACAAGTTGTACAAAAAAGCAGGCTCATGGGTCTCATATGGTTG
LAC4-CDS-2-R	GGGGACCACTTGTACAAGAAAAGCTGGGTCTCCGGTAGTTCTCAGCA
APS4-CDS-1-F	GGGGACAAGTTGTACAGAAAAGCTGGGTCTCCAGCAGAACAGCT
APS4-CDS-2-R	GGGGACAAGTTGTACAGAAAAGCTGGGTCTCCAGCAGAACAGCT
HFRPL18-1-F	GGGGACAAGTTGTACAAAAAAGCAGGCTTATTTTACAACAATTACCAAC
HFRPL18-2-R	GGGGACCACTTGTACAAGAAAAGCTGGGTCTAACCTGAATCCACGACTCTC
P19-2-F	GGGGACAGCTTCTGTACAAAGTGGAACTGGAGCTATAAAGGAAAC
P19-3-R	GGGGACAACCTTGTATAATAAAAGTGGCTATTACTCGCTTCTTCGAAGG
HYL1-CDS-1-F	GGGGACAAGTTGTACAAAAAAGCAGGCTTATGACCTCCACTGATGTTCTCTG
HYL1-CDS-2-R	GGGGACCACTTGTACAAGAAAAGCTGGGTCTCGGTGGCTGCTGTCTCCAC
AGO1-CDS-2-F	GGGGACAGCTTCTGTACAAAGTGGAACTGGAGAAAGAGAACGGATG
AGO1-CDS-3-R	GGGGACAACCTTGTATAATAAAAGTGGCAACGGCATGAAATCAGTGA

qRT-PCR

NAME	SEQUENCE
SPL10-RT-F	GTGGGAGAATGCTCAGGAGGC
SPL10-RT-R	GAGTGTGTTGATCCCTTGTGAATCC
MYB33-RT-F	ATATGGGGCAGTGAAGCTGG
MYB33-RT-R	AGAGTGTGGAGGAGATGACGA
MYB65-RT-F	GATGGTCTGTAGCCATACAGTTAC
MYB65-RT-R	TAGGCATCAACAGAGTCAGGAGATC

ARF17-RT-F	AGCACCTGATCCAAGTCCTTCTATG
ARF17-RT-R	TGGTGAATAGCTGGGGAGGATTTC
CUC1-RT-F	GGAGCACGTGTCCTGTTCT
CUC1-RT-R	GAGCGGGAAAGGAATGTATGA
PHB-RT-F	AGAGTTCCCTTCCAAGGCTACAG
PHB-RT-R	ATAGCGACTATGCCAATAGAACATCC
NF-YA2-RT-F	CTTGAACACTAAAAGTCAGAACTTGG
NF-YA2-RT-R	GACACATTTAATCCGTTGATAAGTT
NF-YA8-RT-F	TCCATATCTGAGCCGGTGGAA
NF-YA8-RT-R	ATCTGGACAAAGCGTGTGAA
TCP4-RT-F	CCTTCAACGACGTCGTTCAGCCAG
TCP4-RT-R	GTGAACCGGTGGAGGAAGGTGATG
APS4-RT-F	GCTGGGCAAGTCCTCTCAAA
APS4-RT-R	CGGAACCGACATGTTGACGA
LAC17-RT-F	CAGACTGAGAGTGAAGCCAGG
LAC17-RT-R	AACCGTGTGATTGCGATGC
AT3G37050-RT-F	TCATGGAGACGCTGCACATT
AT3G37050-RT-R	ATTCCAAAACCTCCCGACCC
CSD2-RT-F	TTTCATCTCCATGAGTTGGTG
CSD2-RT-R	AAAGGCTCTTCCAACAACAGA
ACT2-RT-F	GCACCCCTGTTCTTCTTACCG
ACT2-RT-R	AACCCTCGTAGATTGGCACA
GAPC-RT-F	ACTCAATCACTGCTACTCAG
GAPC-RT-R	GTCAACTTCCGTTAAGAGC

Probe

NAME	SEQUENCE
miR156	GTGCTCACTCTCTCTGTCA
miR158	TGCTTGTCTACATTGGGA
miR159	TAGAGCTCCCTTAATCCAAA
miR160	TGGCATACAGGGAGCCAGGCA
miR162	CTGGATGCAGAGGTTATCGA
miR163	ATCGAAGTTCCAAGTCCTCTCAA
miR164	TGCACGTGCCCTGCTCTCCA
miR165	GGGGGGATGAAGCCTGGTCCGA
miR167	TAGATCATGCTGGCAGCTTCA
miR169	TCGGCAAGTCATCCTGGCTG
miR171	GATATTGGCGCGGCTCAATCA
miR172	ATGCAGCATCATCAAGATTCT
miR395	GAGTTCCCCAACACTTCAG
miR396	CAGTTCAAGAAAGCTGTGGAA
miR398	AAGGGGTGACCTGAGAACACA
miR403	CGAGTTGTGCGTGAATCTAA
miR160c*	GTCAACTTCCGTTAAGAGC

miR165a*	CCTCGATCCAGACAAACATTCC
miR396a*	CTGTATCTTCCCACAGCTTTAT
U6	AGGGGCCATGCTAATCTTCTC

Appendix Table S6. Primers used in this study